J Mol Model (2005) 11: 258–264
DOI 10.1007/s00894-005-0265-6

ORIGINAL PAPER

Peter Politzer · Jane S. Murray · Pat Lane
Monica C. Concha · Ping Jin · Zenaida Peralta-Inga

An unusual feature of end-substituted model carbon (6,0) nanotubes

Received: 9 November 2004 / Accepted: 4 March 2005 / Published online: 12 May 2005

Abstract We have examined the effects of substituents on the computed electrostatic potentials $V_S(\mathbf{r})$ and average local ionization energies $\bar{I}_S(\mathbf{r})$ on the surfaces of model carbon nanotubes of the types (5,5), (6,1) and (6,0). For the (5,5) and the (6,1), the effects upon both $V_S(\mathbf{r})$ and $\bar{I}_S(\mathbf{r})$ of substituting a hydroxyl group at one end are primarily localized to that part of the system. For the (6,0) tube, however, a remarkable change is observed over its entire length, with $V_S(\mathbf{r})$ showing a marked gradation from strongly positive at the substituted end to strongly negative at the other; $\bar{I}_S(\mathbf{r})$ correspondingly goes from higher to lower values. Replacing OH by another resonance- donor, NH_2, produces similar results in the (6,0) system, while the resonance withdrawing NO_2 does the opposite, but in equally striking fashion. We explain these observations by noting that the arrangement of the C−C bonds in the (6,0) tube facilitates charge delocalization over the full length and entire surface of the tube. Substituting NH_2 and NO_2 at opposite ends of the (6,0) tube greatly strengthens the gradations in both $V_S(\mathbf{r})$ and $\bar{I}_S(\mathbf{r})$. The first hyperpolarizability of this system was found to be nine times that of *para*-nitroaniline, suggesting possible nonlinear optical applications.

Keywords Substituted carbon nanotube models · Surface electrostatic potentials · Local ionization energies · Hyperpolarizabilities

Introduction

In two earlier studies [1, 2], we have investigated the computed electrostatic potentials on the inner and outer surfaces of three categories of model nanotubes: carbon; boron/nitrogen, B_xN_x; and carbon/boron/nitrogen, having the stoichiometry $C_{2x}B_xN_x$. The large surface-to-mass ratios of such systems suggest important applications, some of which have already been successful, such as pollutant traps [3], separation of liquid-mixture components [4, 5], catalysts [6] and chemical and biological sensors [7–10], the latter relying upon the fact that adsorption on nanotubes can produce changes in electrical conductivity. All of these applications involve noncovalent interactions with nanotube surfaces, these being primarily electrostatic in nature [11, 12: Chap. 13, 13–15].

We have accordingly characterized the surface electrostatic potentials of a variety of types of model nanotubes [1, 2]: (5,5), (6,0), (8,0), (6,1), (7,1) and (8,1). In all instances, we used structures open at both ends; for the (5,5) and (6,0) nanotubes, we also included the closed forms. We have now begun to look at functionalized systems, with substituents attached to one or both ends of the tube.

In this paper, we report an interesting and significant feature that we have found to be associated with carbon (6,0) systems. Since it appears to have possible applications in optics/electronics areas, we have extended our analysis to include the average local ionization energy as well as the electrostatic potential.

P. Politzer (✉) · J. S. Murray · P. Lane · M. C. Concha
P. Jin · Z. Peralta-Inga
Department of Chemistry,
University of New Orleans, New Orleans,
LA 70148, USA
E-mail: ppolitze@uno.edu

Procedure

The electrostatic potential $V(\mathbf{r})$ that is created at any point in the neighborhood of a molecule by its nuclei and electrons is given by

$$V(\mathbf{r}) = \sum_A \frac{Z_A}{|\mathbf{R}_A - \mathbf{r}|} - \int \frac{\rho(\mathbf{r}')d\mathbf{r}'}{|\mathbf{r}' - \mathbf{r}|} \quad (1)$$

in which Z_A is the charge on nucleus A, located at $\mathbf{R}_A$, and $\rho(\mathbf{r})$ is the molecule's electronic density. $V(\mathbf{r})$ is a physical observable, which can be determined

experimentally, by diffraction techniques [15–17], as well as computationally. Its sign in any given region depends upon whether the positive contribution of the nuclei or the negative one of the electrons is dominant.

The electrostatic potential has been used extensively in analyzing and predicting molecular reactive behavior [15, 17, 18, 19: Chap. 6, 20, 21]; it is particularly effective with respect to noncovalent interactions. For the latter, $V(\mathbf{r})$ is generally computed on the molecular surface, and is labeled $V_S(\mathbf{r})$. We have shown that a variety of properties that depend upon noncovalent interactions (e.g., heats of phase transitions, boiling points and critical constants, partition coefficients and solubilities, hydrogen bonding, etc.) can be expressed quantitatively in terms of certain statistical features of $V_S(\mathbf{r})$; these include its maximum and minimum, average positive and negative values, average deviation and positive and negative variances [22–24]. For these purposes, we take the molecular surface to be the 0.001 electrons/bohr^3 contour of the electronic density, as suggested by Bader et al. [25].

One of the quantities used to characterize $V_S(\mathbf{r})$ that was invoked in this study is the total variance, σ^2_{tot}, which is expressed as the sum of contributions from the positive and negative regions of the surface:

$$\sigma^2_{tot} = \frac{1}{m}\sum_{i=1}^{m}\left[V_S^+(\mathbf{r}_i) - \bar{V}_S^+\right]^2 + \frac{1}{n}\sum_{j=1}^{n}\left[V_S^-(\mathbf{r}_j) - \bar{V}_S^-\right]^2 \qquad (2)$$

In Eq. 2, the summations are over the m positive and n negative points of a square surface grid, with $\bar{V}_S^+$ and $\bar{V}_S^-$ being their averages. σ^2_{tot} is a measure of the variability of $V_S(\mathbf{r})$; it is particularly sensitive to the extrema, because of the terms in Eq. 2 being squared.

The average local ionization energy $\bar{I}(\mathbf{r})$ was defined originally within the framework of Hartree–Fock theory by [26]

$$\bar{I}(\mathbf{r}) = \sum_i \frac{\rho_i(\mathbf{r})|\varepsilon_i|}{\rho(\mathbf{r})} \qquad (3)$$

where $\rho_i(\mathbf{r})$ is the electronic density of the i *th* occupied atomic or molecular orbital, having energy ϵ_i. Invoking Koopmans' theorem [27], which helps justify viewing the $|\epsilon_i|$ as the electronic ionization potentials, $\bar{I}(\mathbf{r})$ is interpreted as the average energy needed to remove an electron at any point $\mathbf{r}$ in the space of an atom or molecule. The focus is upon the point, not upon a particular orbital. Thus the lowest values of $\bar{I}(\mathbf{r})$, the $\bar{I}_{min}$, indicate the sites of, on the average, the most energetic and readily transferred electrons.

$\bar{I}(\mathbf{r})$ has been shown to be related to atomic shell structure [28], local polarizability in molecules [29, 30], local temperature [31] and bond strain [32]. When computed on a molecular surface, $\bar{I}_S(\mathbf{r})$, it is also an effective guide to reactivity toward electrophiles [26, 33–36], this being greatest where $\bar{I}_S(\mathbf{r})$ has its minima, the $\bar{I}_{S,min}$ It has been shown that the $\bar{I}_{S,min}$. coming from Kohn–Sham density functional procedures are as reliable for this purpose as are the Hartree–Fock [34].

In this work, we have optimized the geometries and computed $V_S(\mathbf{r})$ and $\bar{I}_S(\mathbf{r})$ for several model carbon nanotubes with the Gaussian 03 code [37], at the Hartree–Fock (HF) STO-5G//STO-3G level. The use of a minimum basis set was dictated by the sizes of the systems. However, we confirmed, in a test case, that density functional B3PW91/6-31G* calculations produce the same key features. It has also been demonstrated, by us [38] and by others [21], that minimum basis sets are satisfactory for our present objectives. All of the tubes included in this study are open at both ends. We followed the common procedure of using hydrogens to satisfy the unfulfilled valencies [39–44].

Results and discussion

Figure 1 shows the structural frameworks of the three carbon model nanotubes upon which we are focusing. They are of types (5,5), (6,1) and (6,0). In Figs. 2a, 3a and 4a are the computed electrostatic potentials on their outer surfaces (which are taken to be the 0.001 electrons/bohr^3 contours of the electronic density on the outside of each tube). The general features of these $V_S(\mathbf{r})$ are fully consistent with what we found earlier for related systems [1, 2]. Closed carbon tubes are very weakly positive over most of their outer surfaces, negative regions being

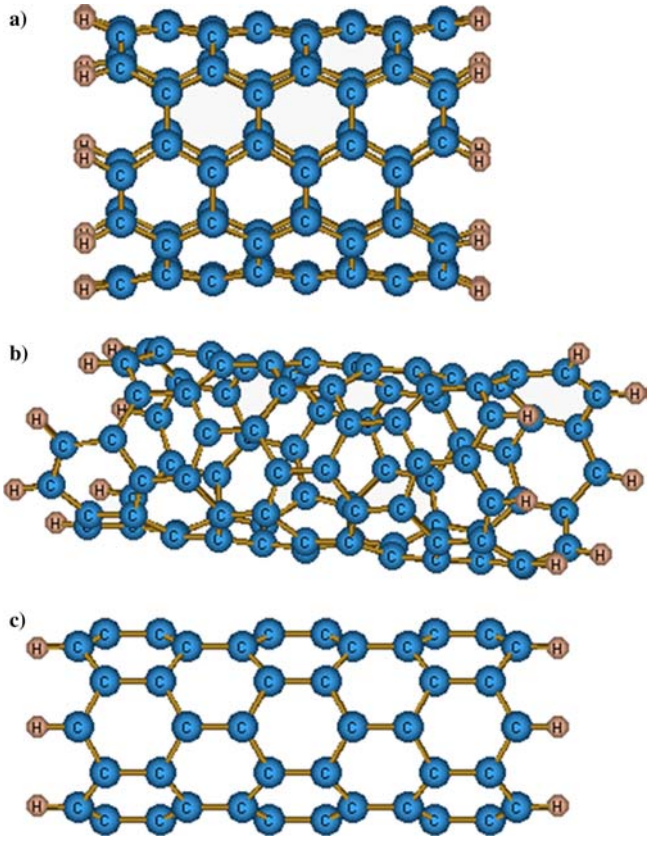

Fig. 1 Three-dimensional structures of: **a** (5,5) $C_{80}H_{20}$, **b** (6,1) $C_{68}H_{14}$ and **c** (6,0) $C_{72}H_{12}$

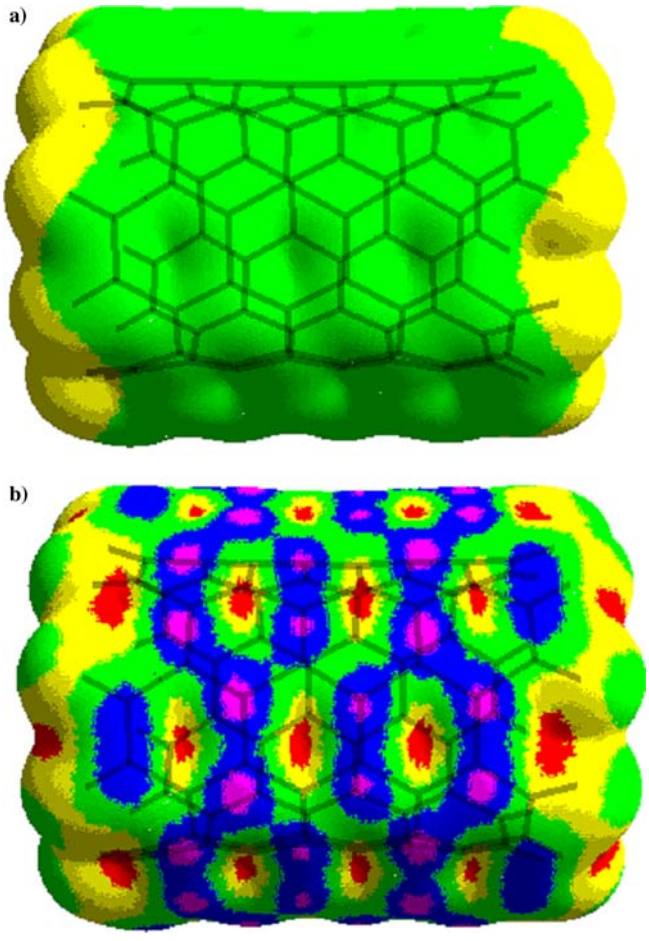

Fig. 2 HF/STO-5G electrostatic potential **(a)** and average local ionization energy **(b)** on outer surface of open (5,5) $C_{80}H_{20}$. Color ranges: **a** In kcal mol^{-1} : *green* is between −10 and 0 and *yellow* is between 0 and 15. **b** In eV: *purple* is less than 14, *blue* is between 14 and 15, *green* is between 15 and 16.5, *yellow* is between 16.5 and 17.5, and *red* is more than 17.5

primarily at the more highly curved ends. The terminal hydrogens of the open systems provide some electronic charge to the carbon portions and these become slightly negative. The inner surfaces are invariably somewhat more positive (or less negative) than the outer, due to the closer proximity of more nuclei. However the dominant theme in carbon nanotube $V_S(\mathbf{r})$, particularly on the side walls, is near-zero weakness and blandness, showing relatively little variation (certain caps with high curvature can somewhat modify this picture [45]).

This generalization can be quantified by considering the values of σ^2_{tot}, listed in Table 1. For the (5,5), (6,1) and (6,0) systems, σ^2_{tot} is quite small, in the neighborhood of 20 (kcal mol^{-1})^2 . To put this in perspective, its values for some representative organic molecules are also given in Table 1. With the exception of the hydrocarbons, they are considerably larger, usually by an order of magnitude. This shows that the surface electrostatic potentials of these molecules are much stronger and more variable than are those of the unsubstituted nanotubes.

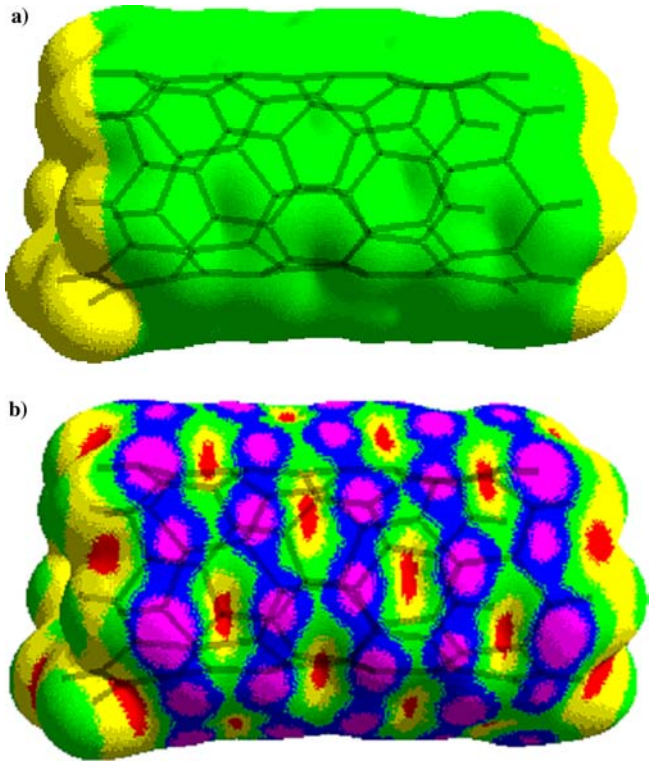

Fig. 3 HF/STO-5G electrostatic potential **(a)** and average local ionization energy **(b)** on outer surface of open (6,1) $C_{68}H_{14}$. Color ranges are the same as in Fig. 2

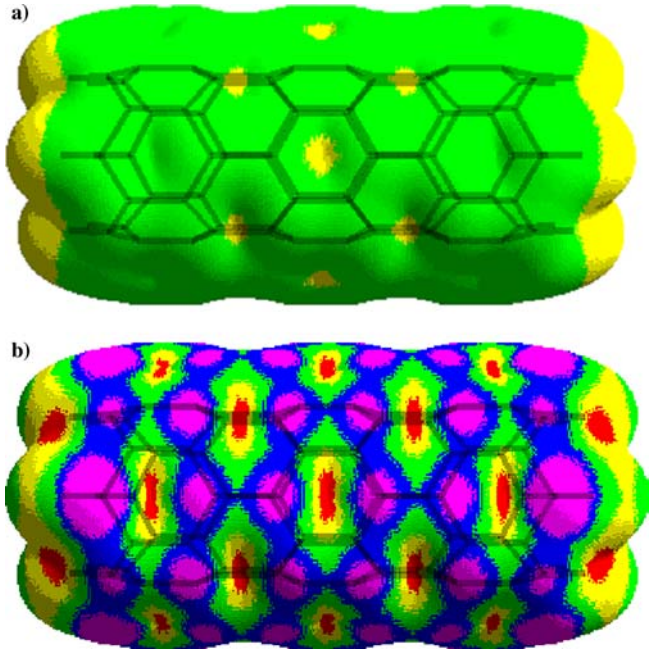

Fig. 4 HF/STO-5G electrostatic potential **(a)** and average local ionization energy **(b)** on outer surface of open (6,0) $C_{72}H_{12}$. Color ranges are the same as in Fig. 2

More interesting are the average local ionization energies on the tube surfaces, in Figs. 2b, 3b and 4b. These show regular patterns of high and low $\bar{I}_S(\mathbf{r})$, with

Table 1 Computed total variances on surfaces of model nanotubes and representative organic molecules

System		σ^2_{tot}(kcal mol^{-1})^2
Model nanotubes[a]		
$C_{80}H_{20}$	(5,5)	19.3
$C_{68}H_{14}$	(6,1)	21.1
$C_{72}H_{12}$	(6,0)	22.2
$C_{80}H_{19}OH$	(5,5)	46.0
$C_{68}H_{13}OH$	(6,1)	60.7
$C_{72}H_{11}OH$	(6,0)	419.1
$C_{72}H_{11}NH_2$	(6,0)	548.7
$C_{72}H_{11}NO_2$	(6,0)	933.3
$H_2NC_{72}H_{10}NO_2$	(6,0)	1036.1
Representative molecules[b]		
C_2H_6		4.0
Naphthalene		15.9
C_6H_6		16.3
C_2F_6		73.1
Indole		96.6
CH_3NO_2		116.0
CH_3COOCH_3		138.9
$(CH_3)_2O$		173.7
C_6H_5CN		195.3
C_2H_5OH		227.5
$(CH_3)_2NH$		241.2
H_2NCHO		319.1

[a] The σ^2_{tot} for $C_{80}H_{20}$ and $C_{68}H_{14}$ are from Ref. [2]; those for the other model nanotubes are from the present work.
[b] Reference [22].

minima $(\bar{I}_{S,min})$ above the carbons. (In an analogous study of some models of graphene, which is a two-dimensional sheet of graphite, $\bar{I}_{S,min}$ were observed above all of the interior carbons [46].)

The $\bar{I}_{S,min}$ in Figs. 2b, 3b and 4b are in the general neighborhood of 13 eV. For comparison, the HF/STO-5G $\bar{I}_{S,min}$ in benzene, which are located above each carbon, are 14.3 eV [46]. (Since an $\bar{I}_{S,min}$ does reflect some probability of inner electrons being at the site in question, it tends to be larger than the magnitude of the highest occupied orbital energy or the measured first ionization potential.)

In Figs. 5, 6 and 7 are seen the consequences of substituting a hydroxyl group, OH, at one end of each tube. In each instance, it is essentially in the plane of the ring to which it is attached. For the (5,5) and (6,1) systems, the effects are fairly localized. There are, as anticipated, strong positive and negative electrostatic potentials associated with the hydroxyl hydrogen and oxygen, respectively, which result in σ^2_{tot} being more than doubled (Table 1). There is also a significant increase in $\bar{I}_S(\mathbf{r})$ in the vicinity of the OH, due to the higher ionization energy of oxygen compared to carbon. However, the remainder of each tube, in the case of the (5,5) and the (6,1), is relatively little affected by the substitution of OH. Compare Figs. 2 and 5 and Figs. 3 and 6.

The situation is strikingly different for the (6,0) system (Fig. 7). The introduction of OH produces a gradation of $V_S(\mathbf{r})$ along the entire length of the tube, from strongly positive at the substituted end to strongly negative at the other. σ^2_{tot} increases to 419.8 (kcal mol^{-1})^2. The effect upon $\bar{I}_S(\mathbf{r})$ is not quite as pronounced, but

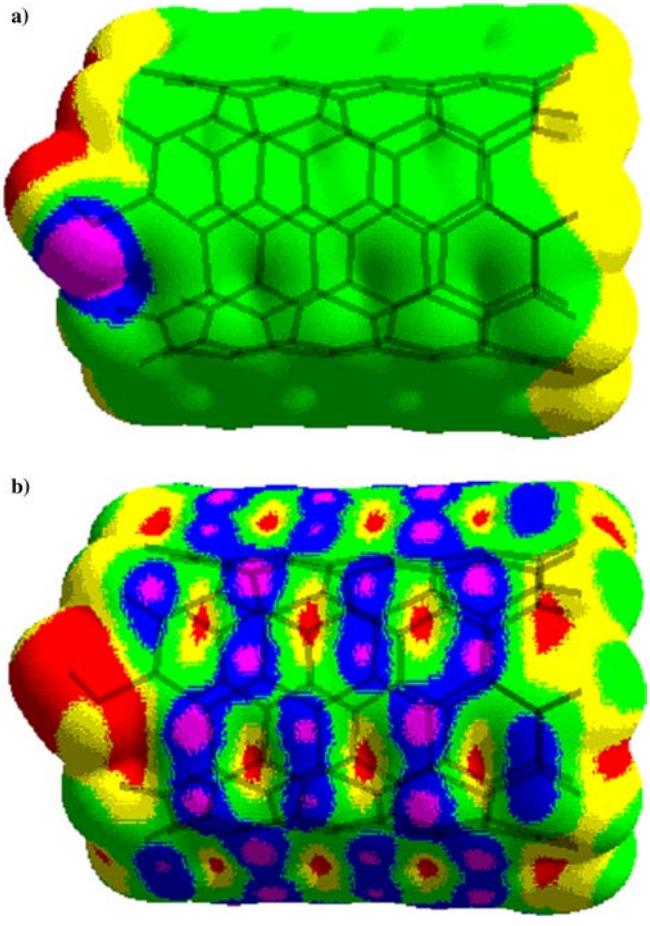

Fig. 5 HF/STO-5G electrostatic potential **(a)** and average local ionization energy **(b)** on outer surface of open (5,5) $C_{80}H_{19}OH$. The hydroxyl group is at the left end of the tube. Color ranges: **a** In kcal mol^{-1}: *purple* is more negative than −20, *blue* is between −20 and −10, *green* is between −10 and 0, *yellow* is between 0 and 15, and *red* is greater than 15. **b** In eV: *purple* is less than 14, *blue* is between 14 and 15, *green* is between 15 and 16.5, *yellow* is between 16.5 and 17.5, and *red* is more than 17.5

there is clearly a marked tube-long trend from higher to lower values in moving away from the OH.

We explain these dramatic differences between the surface properties of the (6,0) tube and those of the (5,5) and (6,1) by invoking their structures, shown in Fig. 1. Only the (6,0) has alternate C−C bonds parallel to the tube axis, which permits maximum 2pπ–2pπ overlap. The (5,5) and (6,1) have no C−C bonds in which such overlap is not impeded, at least somewhat, by the curvature of the side walls. The hydroxyl group is a strong resonance provider of electronic charge [47], and the arrangement of bonds, in conjunction with the high polarizability of carbon nanotubes [48–50], allows delocalization of the donated charge parallel to the tube axis over the full length of the tube (Scheme 1). The influence of a single OH is felt over the entire surface. (Inductively, the hydroxyl group is a charge withdrawer [47]. In the present case, however, the resonance effect is clearly dominant.)

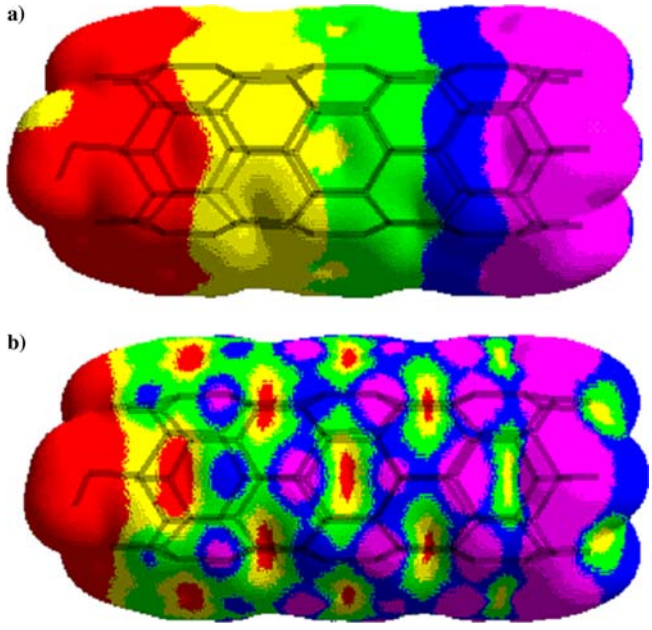

Fig. 6 HF/STO-5G electrostatic potential **(a)** and average local ionization energy **(b)** on outer surface of open (6,1) $C_{68}H_{13}OH$. The hydroxyl group is at the left end of the tube. Color ranges are the same as in Fig. 5

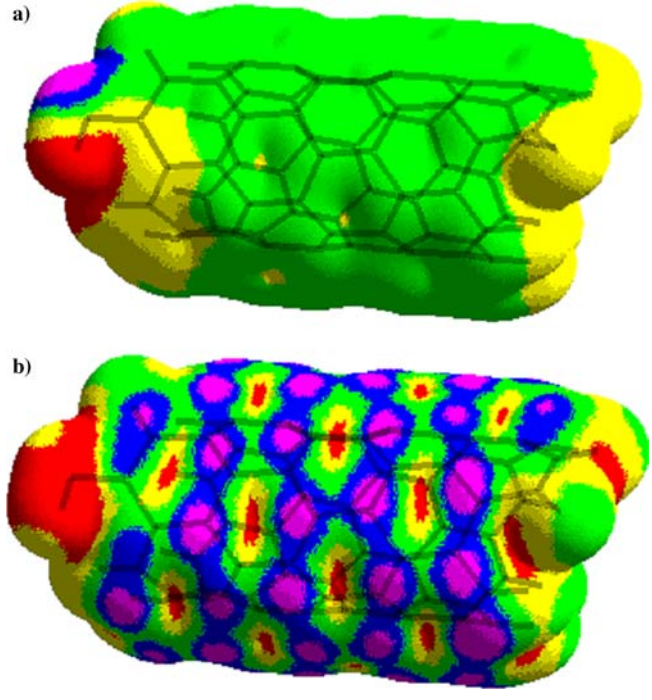

Fig. 7 HF/STO-5G electrostatic potential **(a)** and average local ionization energy **(b)** on outer surface of open (6,0) $C_{72}H_{11}OH$. The hydroxyl group is at the left end of the tube. Color ranges are the same as in Fig. 5

In order to investigate this (6,0) delocalization further, we tested two other substituents, the resonance donor NH_2 and the resonance withdrawer NO_2. For

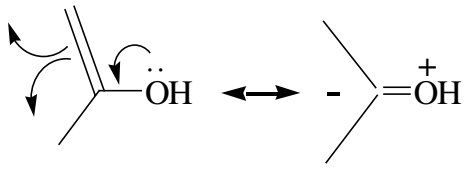

Sch. 1 Impetus for charge delocalization in (6,0) nanotube end-substituted by OH

NH_2, the $V_S(\mathbf{r})$ and $\bar{I}_S(\mathbf{r})$ patterns are similar to those for OH; σ^2_{tot} equals 548.7 $(\text{kcal mol}^{-1})^2$. For NO_2, sharp gradations in $V_S(\mathbf{r})$ and $\bar{I}$ are also obtained, but in the opposite sense. The substituted end has strongly negative electrostatic potentials, with low $\bar{I}_S(\mathbf{r})$, while the other end is strongly positive and has high $\bar{I}_S(\mathbf{r})$ (Fig. 8). $\sigma^2_{tot} = 933.4$ $(\text{kcal mol}^{-1})^2$. This can again be explained by charge delocalization, driven by the electron-withdrawing NO_2 (Scheme 2).

Supporting our interpretation, and Schemes 1 and 2, are the optimized HF/STO-3G C–OH, C–NH_2 and C–NO_2 distances in these model nanotubes, 1.361, 1.350 and 1.454 Å, respectively. They are considerably shorter than is typical for such single bonds, as in $(H_3C)_2CH–OH$ (1.438 Å), $(H_3C)_2CH–NH_2$ (1.491 Å) and $(H_3C)_2CH–NO_2$ (1.545 Å).

It is well known that a molecule with donor and acceptor groups linked by a conjugated bridge may have significant nonlinear optical properties [51–55]. By this are generally meant the effects arising from the second- and third-order terms in the Taylor series expansion showing how the molecule's dipole moment is affected

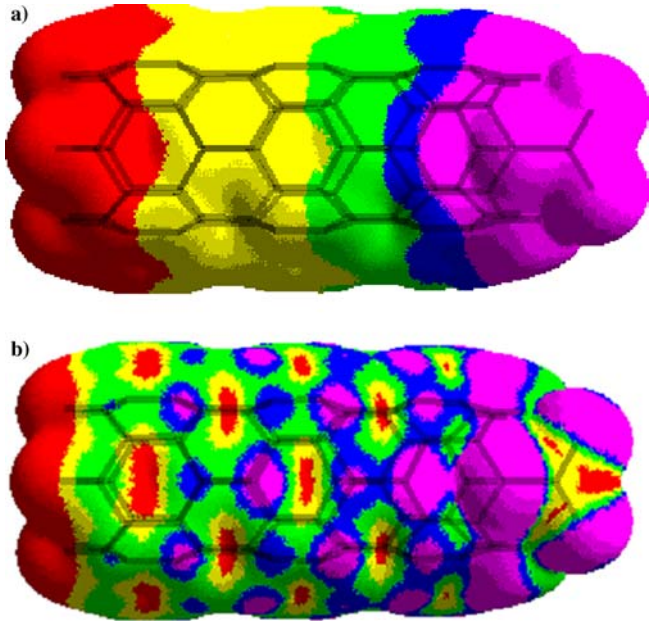

Fig. 8 HF/STO-5G electrostatic potential **(a)** and average local ionization energy **(b)** on outer surface of open (6,0) $C_{72}H_{11}NO_2$. The nitro group is at the right end of the tube. Color ranges are the same as in Fig. 5

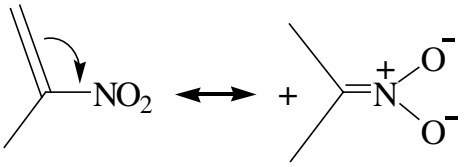

Sch. 2 Impetus for charge delocalization in (6,0) nanotube end-substituted by NO_2

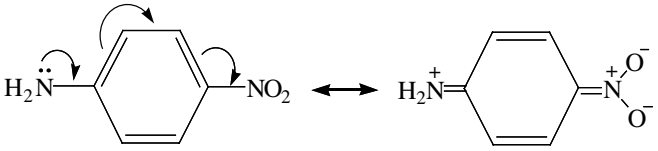

Sch. 3 Charge delocalization in *para*-nitroaniline

by the oscillating electric field of electromagnetic radiation:

$$\mu_i(\varepsilon) = \mu_i(0) + \sum_j \alpha_{ij}\varepsilon_j + \frac{1}{2}\sum_{jk}\beta_{ijk}\varepsilon_j\varepsilon_k + \frac{1}{6}\sum_{jkm}\gamma_{ijkm}\varepsilon_j\varepsilon_k\varepsilon_m + \cdots \quad (4)$$

In Eq. 4, the indices refer to components along different axes. The tensors α, β and γ are designated, respectively, the polarizability and the first and second hyperpolarizabilities.

The large increase in dipole moment that accompanies the charge transfer transition in molecules having donor and acceptor groups connected through a conjugated system reflects enhanced second- and third-order (i.e., nonlinear) contributions to μ_i (ϵ) [51–53, 55]. This occurs, for example, in the prototypical *para*-nitroaniline (see Scheme 3).

The resulting nonlinear response to electromagnetic radiation can have a variety of potentially important applications, for instance, in frequency converters, electrooptic modulators and optical switches [51, 56, 57: Chap. C2.15]. The bulk phase analogue of Eq. 4 relates the field-dependent polarization of the material to its first-, second- and third-order susceptibilities, $\chi^{(1)}$, $\chi^{(2)}$ and $\chi^{(3)}$, which replace α, β and γ.

These considerations, in conjunction with our observation of the remarkable delocalization in substituted model carbon (6,0) nanotubes, suggested that we investigate the consequences of having an NH_2 (donor) and an NO_2 (acceptor) at opposite ends of the tube. Figure 9 confirms that this reinforces and strengthens the gradations in $V_S(\mathbf{r})$ and $\bar{I}_S(\mathbf{r})$,and their extrema at the tube ends. σ^2_{tot} increases to 1,036.1 (kcal mol^{-1})^2, which is among the largest values that we have ever encountered. (Comparable ones were found for tautomeric zwitterions of glycine and histidine [58].) We also used Gaussian 03 to compare the predicted first hyperpolarizabilities β of *para*-nitroaniline, Scheme 3, and the (6,0) tube in Fig. 9. At the local density functional SVWN/6-31G* level, β is greater for the latter, by a factor of 9. These findings introduce the possibility of appropriately substituted carbon (6,0) nanotubes serving as nonlinear optical materials. There have already been extensive studies of optical nonlinearity in fullerenes and non-functionalized nanotubes [54, 59–63].

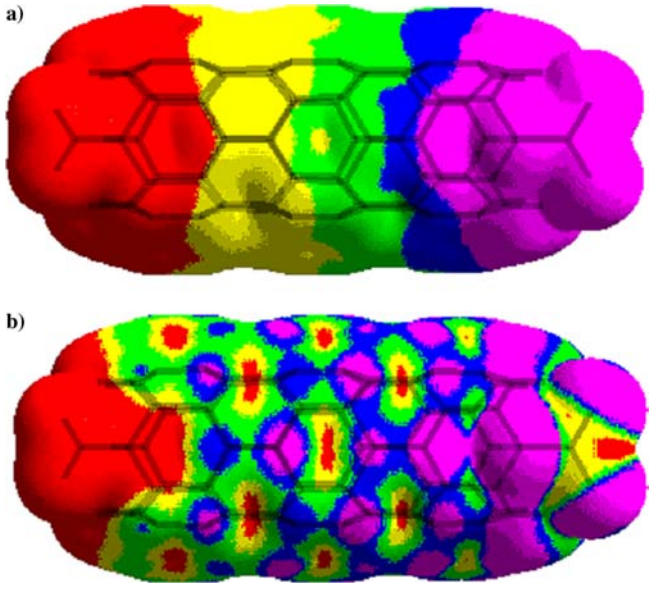

Fig. 9 HF/STO-5G electrostatic potential **(a)** and average local ionization energy **(b)** on outer surface of open (6,0) $C_{72}H_{10}NH_2NO_2$. The nitro group is at the right end of the tube, the amino group at the left. Color ranges are the same as in Fig. 5

Summary

When our carbon (6,0) tube is functionalized at one end with either a donor or an acceptor group, there results a striking gradation in both the electrostatic potential and the average local ionization energy on its surface, extending its full length. One end has strongly positive $V_S(\mathbf{r})$ and high $\bar{I}_S(\mathbf{r})$, the other has the opposite. These features are reinforced when both a donor and an acceptor are present. We have not found such behavior in tubes of other (*n, m*) types.

A number of points need to be addressed in future work. Preliminary studies of (8,0) systems indicate, as anticipated, that delocalization occurs in these as well; they do have the same type of bond structure as the (6,0). However, the (8,0) tube diameter is larger, which is reflected in the surface potentials being somewhat weaker, although still showing a gradation from positive to negative along the length of the tube. The effects of tube diameter and length, for different (*n*,0) types, should be explored.

Finally, what will be the result of introducing additional substituents, and varying their orientations relative to the tube axes? One limiting case would be to replace all of the hydrogens, by donor groups at one end

and acceptors at the other. This could be particularly relevant to potential nonlinear optical applications.

References

1. Peralta-Inga Z, Lane P, Murray JS, Boyd S, Grice ME, O'Connor CJ, Politzer P (2003) Nano Lett 3:21–28
2. Politzer P, Lane P, Murray JS, Concha MC (in press) J Mol Model
3. Long RW, Yang RT (2001) J Am Chem Soc 123:2058–2059
4. Mao Z, Sinnott SB (2001) J Phys Chem B 105:6916–6924
5. Peng X, Li Y, Luan Z, Di Z, Wang H, Tian B, Jia Z (2003) Chem Phys Lett 376:154–158
6. Halls MD, Schlegel HB (2002) J Phys Chem B 106:1921–1925
7. Kong J, Franklin NR, Zhou C, Chapline MG, Peng S, Cho K, Dai H (2000) Science 287:622–625
8. Goldoni A, Larciprete R, Petaccia L, Lizzit S (2003) J Am Chem Soc 125:11329–11333
9. Chen RJ, Bangsaruntip S, Drouvalakis KA, Wong Shi Kam N, Shim M, Li Y, Kim W, Utz PJ, Dai H (2003) Proc Natl Acad Sci USA 100:4984–4989
10. Chen RJ, Choi HC, Bangsaruntip S, Yenilmez E, Tang X, Wang Q, Chang Y-L, Dai H (2004) J Am Chem Soc 126:1563–1568
11. Feynman RP (1939) Phys Rev 56:340–343
12. Hirschfelder JO, Curtiss CF, Bird RB (1954) Molecular theory of gases and liquids. Wiley, New York
13. Hirschfelder JO, Meath WJ (1967) Adv Chem Phys 12:3–106
14. Buckingham AD (1967) Adv Chem Phys 12:107–142
15. Naray-Szabo G, Ferenczy GG (1995) Chem Rev 95:829–847
16. Stewart RF (1972) J Chem Phys 57:1664–1668
17. Politzer P, Truhlar DG (eds) (1981) Chemical applications of atomic and molecular electrostatic potentials. Plenum, New York
18. Scrocco E, Tomasi J (1978) Adv Quantum Chem 11:115–193
19. Politzer P, Daiker KC (1981) In: Deb BM (ed) The force concept in chemistry. Van Nostrand Reinhold, New York
20. Politzer P, Laurence PR, Jayasuriya K (1985) Environ Health Perspect 61:191–202
21. Politzer P, Murray JS (1991) Rev Comput Chem 2:273–312
22. Murray JS, Politzer P (1998) J Mol Struct (Theochem) 425:107–114
23. Politzer P, Murray JS (1999) Trends Chem Phys 7:157–168
24. Politzer P, Murray JS (2001) Fluid Phase Equilib 185:129–137
25. Bader RFW, Carroll MT, Cheeseman JR, Chang C (1987) J Am Chem Soc 109:7968–7979
26. Sjoberg P, Murray JS, Brinck T, Politzer P (1990) Can J Chem 68:1440–1443
27. Koopmans TA (1933) Physica 1:104–113
28. Politzer P, Murray JS, Grice ME, Brinck T, Ranganathan S (1991) J Chem Phys 95:6699–6704
29. Jin P, Brinck T, Murray JS, Politzer P (2003) Int J Quantum Chem 95:632–637
30. Jin P, Murray JS, Politzer P (2004) Int J Quantum Chem 96:394–401
31. Nagy A, Parr RG, Liu S (1996) Phys Rev A 53:3117–3121
32. Murray JS, Seminario JM, Politzer P, Sjoberg P (1990) Int J Quantum Chem Quantum Chem Symp 24:645–653
33. Brinck T, Murray JS, Politzer P (1993) Int J Quantum Chem 48:73–88
34. Politzer P, Abu-Awwad F, Murray JS (1998) Int J Quantum Chem 69:607–613
35. Murray JS, Peralta-Inga Z, Politzer P, Ekanayake K, LeBreton P (2001) Int J Quantum Chem 83:245–254
36. Politzer P, Murray JS, Concha MC (2002) Int J Quantum Chem 88:19–27
37. Frisch MJ, Trucks GW, Schlegel HB, Scuseria GE, Robb MA, Cheeseman JR, Zakrezewski VG, Montgomery JA, Stratmann RE, Burant JC, Dappich S, Millam JM, Daniels AD, Kudin KN, Strain MC, Farkas O, Tomasi J, Barone V, Cossi M, Cammi R, Mennucci B, Pomelli C, Adamo C, Clifford S, Ochterski J, Petersson G, Aayala PY, Cui Q, Morokuma K, Malick DK, Rubuck AD, Raghavachari K, Foresman JB, Cioslowski J, Ortiz JV, Stefanov BB, Liu G, Liashenko A, Piskorz P, Komaromi I, Gomperts R, Martin RL, Fox D J, Keith T, Al-Laham MA, Peng CY, Nanayakkara A, Gonzalez C, Challacombe M, Gill PMW, Johnson BG, Chen W, Wong MW, Andres JL, Head-Gordon M, Replogle ES, Pople JA (2003) Gaussian 03. Gaussian Inc, Pittsburgh PA
38. Murray JS, Brinck T, Politzer P (1992) J Mol Struct (Theochem) 255:271–281
39. Mazzoni MSC, Chacham H, Ordejon P, Sanchez-Portal D, Soler JM, Artacho E (1999) Phys Rev B 60:R2208–R2211
40. Bauschlicher CW Jr (2001) Nano Lett 1:223–226
41. Halls MD, Schlegel HB (2002) J Phys Chem B 106:1921–1925
42. Irle S, Mews A, Morokuma K (2002) J Phys Chem A 106:11973–11980
43. Jaffe RL (2003) J Phys Chem B 107:10378–10388
44. Zhou Z, Steigerwald M, Hybertsen M, Brus L, Friesner RA (2004) J Am Chem Soc 126:3597–3607
45. Politzer P, Lane P, Concha MC, Murray JS (in press) Microelectron Eng
46. Peralta-Inga Z, Murray JS, Grice ME, Boyd S, O'Connor CJ, Politzer P (2001) J Mol Struct (Theochem) 549:147–158
47. Exner O (1988) Correlation analysis of chemical data. Plenum, New York
48. Benedict LX, Louie SG, Cohen ML (1995) Phys Rev B 52:8541–8549
49. Wan X, Dong J, Xing DY (1998) Phys Rev B 58:6756–6759
50. Jensen L, Astrand P-O, Mikkelsen KV (2004) J Phys Chem A 108:8795–8800
51. Williams DJ (1984) Angew Chem Int Ed Engl 23:690–703
52. Beratan DN (1991) In: Marder SR, Sohn JE, Stucky GD (eds) New materials for nonlinear optics, vol 455. ACS Symposium Series. American Chemical Society, Washington, DC, pp89–102
53. Kanis DR, Ratner MA, Marks TJ (1994) Chem Rev 94:195–242
54. Bredas JL, Adant C, Tackx P, Persoons A, Pierce BM (1994) Chem Rev 94:243–278
55. Matsuzawa N, Dixon DA (1994) J Phys Chem 98:2545–2554
56. Karna SP (2000) J Phys Chem A 104:4671–4673
57. Wilson WL (2001) In: Moore JH, Spencer ND (eds) Encyclopedia of chemical physics and physical chemistry, vol III. Institute of Physics, London
58. Murray JS, Peralta-Inga Z, Politzer P (2000) Int J Quantum Chem 80:1216–1223
59. Liu X, Si J, Chang B, Xu G, Yang Q, Pan Z, Xie S, Ye P, Fan J, Wan M (1999) Appl Phys Lett 74:164–166
60. Jiang J, Dong J, Xing DY (1999) Phys Rev B 59:9838–9841
61. Slepyan GYa, Maksimenko SA, Kalosha VP, Herrmann J, Campbell EEB, Hertel IV (1999) Phys Rev A 60:R777–R780
62. Chen P, Wu X, Sun X, Lin J, Ji W, Tan KL (1999) Phys Rev Lett 82:2548–2551
63. Mishra SR, Rawat HS, Mehendale SC, Rustagi KC, Sood AK, Bandyopadhyay R, Govindaraj A, Rao CNR (2000) Chem Phys Lett 317:510–514